MICROSTRUCTURE OF ALUMINUM HYDRIDE AND STABILIZATION CONCEPTS

Michael Herrmann, Ulrich Förter-Barth, Hubert Weyrauch,
Mar Juez Lorenzo, and Paul Bernd Kempa

Fraunhofer Institut für Chemische Technologie ICT, D-76327 Pfinztal, Germany
e-mail to michael.herrmann@ict.fraunhofer.de

Introduction

Aluminum hydride (AlH_3, alane) is a promising substance for hydrogen and energy storage systems, rocket propellants, and space applications [e. g. 1–4]. The substance is sensitive against humidity and oxidation, and will decompose in air and water, although passivation greatly diminishes the decomposition rate [5]. A high stability variant was produced in former Soviet Russia and was even used in the ballistic missiles SS-24. The material is however not commercially available, and details of the synthesis and production (stabilization) are unknown [6]. Investigations of this product at the Fraunhofer ICT in the early 2000s revealed interesting details, but no conclusive stabilization concepts [7, 8]. With rising new interest for applications of alane in solid rocket propellants at the Fraunhofer ICT, e. g. due to a potential increase of the specific impulse of ADN/GAP propellants by about 10 %, new structure investigations were restarted with modern characterization technologies available today. Besides, new literature contributions have been reviewed including stabilization mechanisms, related microstructures and alane provider [9]. The investigations revealed new structural aspects and stabilization concepts.

Samples, experimental and evaluation

A white (slightly purple) alane powder was received in the year 2002 with the charge specification aluminum hydride hydroreactive GAL-2. For comparison, a nanometer-sized aluminum (ALEX), a micron sized aluminum and an aluminum oxide sample from Fraunhofer ICT stock were added to the sample portfolio. The surface topography was investigated using

a confocal microscope μsurf custom from NanoFokus AG, equipped with a 505 nm LED light source and a CCD camera. Alane particles were glued with a thermoplastic adhesive (Tempfix) at 50 °C on a sample holder. Height profiles of selected defective surface sections with sub-micrometer resolution were evaluated with the contact-free surface metrology. For comparison, the same crystals were also inspected with the scanning electron microscope (SEM) with 10 kV electrode voltage. Energy-dispersive X-ray spectroscopy (EDX) was performed in vacuum on a microprobe EDAX32. Therefore, alane particles were fixed with an adhesive on a palladium sample holder and were sputtered with gold. The voltage of the primary electrode varied between 5 and 20 kV, and the measuring times were extended up to 317 s. For comparison, further measurements were performed with an SEM EVO MA 010 from Zeiss equipped with an EDS X-Max50 silicon-drift detector (SDD) from Oxford Instrument and samples were fixed again with the thermoplastic adhesive (Tempfix).

X-ray diffraction (XRD) patterns were measured with a Bragg-Brentano diffractometer, D8 Advance from Bruker AXS, equipped with copper tube, nickel K_β-filter, two 2.5° Soller collimators, variable V6 divergence slit, a temperature device from MRI, and a silicon-strip detector (LynxEye) with 3 °2θ detector opening. Long term patterns were measured between 5 and 100 °2θ with 0.02 °2θ step width and 10 s counting time per step (14 h/pattern). Temperature resolved series were measured while samples were heated or cooled stepwise between –70 and 200 °C under nitrogen flushing. The patterns were captured between 10 and 80 °2θ with 0.05 °2θ step width and 3 s counting time per step (~70 min/pattern). The diffraction patterns were evaluated by means of Rietveld analysis [10] using the program TOPAS from Bruker AXS [11], and crystallographic parameters, such as crystal phase, cell volume and thermal linear expansion coefficients, were determined.

Results

Surface topography – SEM and confocal microscopy

Figure 1 depicts selected SEM pictures with a well crystallized (euhedral) particle (left) and a defective particle (middle) with fissures or perforations along grain boundaries or slip-planes. Surface ditches most likely represent end points of internal linear defects, such as dislocations, piling up in slip planes. Corrosion started at these defects and penetrated the crystal. Re-

evaluation of older recordings of the same lot revealed similar defects, but also strongly eroded crystals with pitting corrosion (right). Most likely highly defective crystals disappeared gradually over the years, and thus were not observed in the new SEM pictured in high concentration. The hollowing of particles proves that the crystal faces are the stable part and prevent the structure from decomposition if no crystal defects perforate the particle surface. The metrology of a selected defective crystal faces with height profiles is shown in Figure 2.

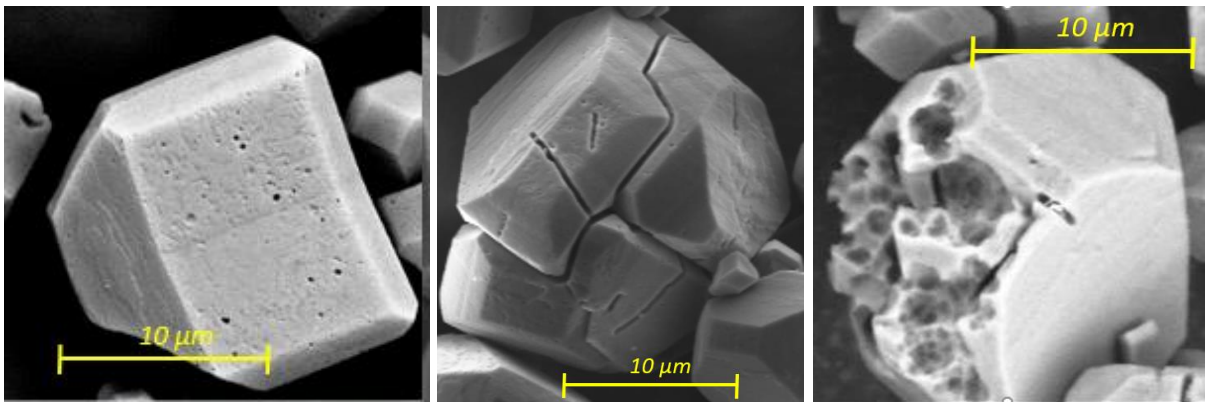

Figure 1: SEM images of alane crystals and defects (GAL-2). Euhedral crystal (left), ditches along grain boundaries or dislocation slip-planes (middle) and strongly corroded (hollowed) crystal (right).

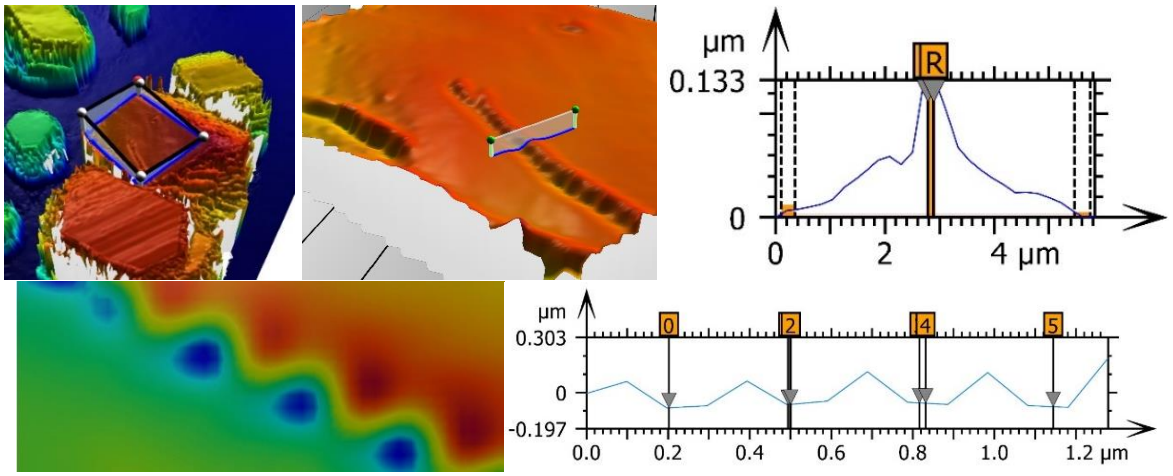

Figure 2: Selected surface section (top left and middle) with two surface perforations, 2D false-color image of a defective surface section (bottom left), and related height profiles (right).

Two fissures with slightly bulged edges appeared on the surface section. Maximum height differences in the profiles reached 0.6 to 1.3 µm. Furthermore, a periodicity along the fissure was found, with ditch distances between 0.29 and 0.32 µm. However, it is not clear yet, whether the periodic patterns represent perforations or arose from measuring or preparation effects,

such as interferences. Further investigations e. g. with atomic force microscopy shall answer this question. In total, the investigations support the hypothesis that surface defects origin from intrinsic lattice defects, such as grain boundaries and dislocations or twin-planes. Detailed data of the topographic investigations will be reported elsewhere.

Elemental analysis (EDX)

Signals of gold and palladium (from the sputtering process and sample holder) and carbon (from the glue) are visible beside aluminum and oxygen in EDX spectra of the alane sample (Figure 3 left). The 2D superposition image of the concentrations of aluminum, oxide, and carbon on the right side of the figure depicts a homogeneous distribution over the particles. No concentration of elements at distinct crystal positions, such as edges or defective areas, were detected. Thus, the investigations even with increased resolution and elongated measuring times verify the absence of stabilization additives, such as magnesium.

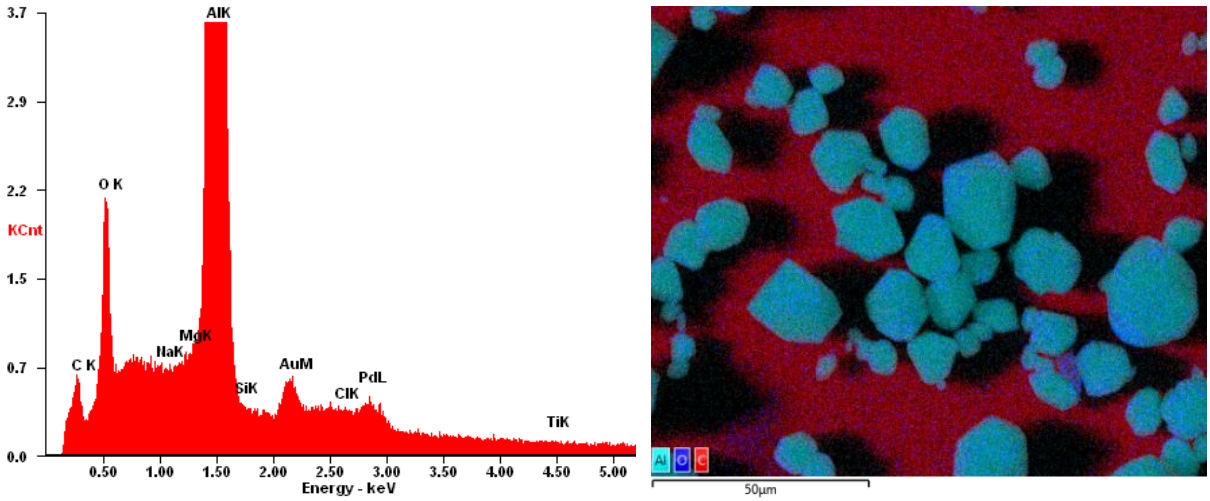

Figure 3: EDX spectrum of alane. No unexpected signals were detected (left) and EDX-superposition image (right) of the concentrations of aluminum (cyan), oxygen (purple), and carbon (magenta).

X-ray diffraction

In the diffraction pattern of the alane (Figure 4) red reference markers identify the expected aluminum hydride phase α (ICDD, PDF 23-0761). Besides, the long-term measurement revealed interesting details of the underground, such as the absorption edge of the K_β-Filter and the exponentially decreasing bremsstrahlung emerging under the large peaks (small

diagram). These edge-maxima may be misinterpreted as extrinsic diffraction peaks or phases. More interesting are small peaks that emerge in the background, some may belong to other aluminum hydride polymorphs (PDF 39-0758, Figure 5) or aluminum hydroxide (PDF 26-0025).

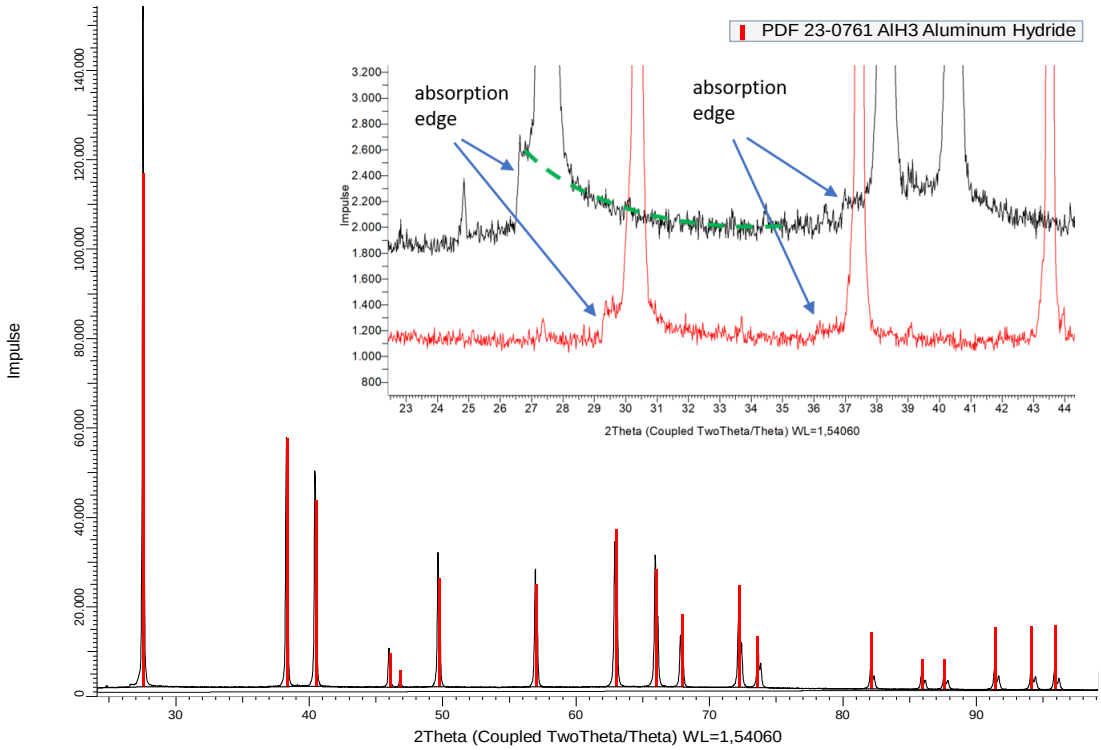

Figure 4: XRD pattern of alane (black) and reference markers (red) of the α-phase of aluminum hydride (PDF 23-0761 [12]) and enlarged view of the background (small window). With the high counting rates of the detector the absorption edge of the Kβ filter and exponentially decreasing bremsstrahlung (green dashed line) emerge under strong diffraction peaks.

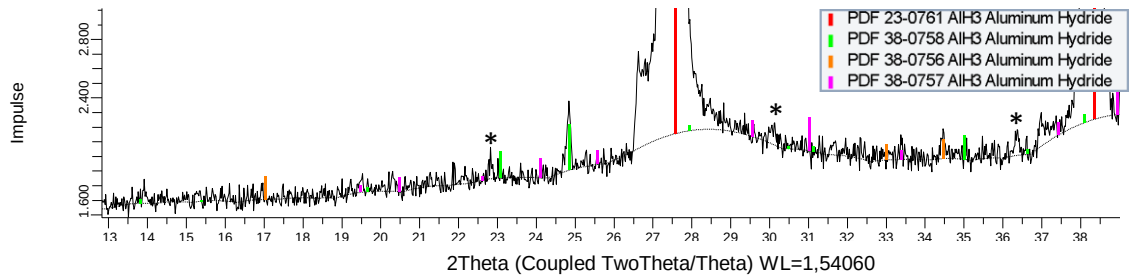

Figure 5: Part of a diffraction pattern of alane with reference markers of the aluminum hydride polymorphs. Beside the α-phase (red markers) a low concentration of further polymorph (green) was detected. Further unidentified peaks are marked with asterisks.

Temperature-resolved investigations

In the waterfall plot of the temperature cycle of alane in Figure 6 α-AlH_3 (PDF 23-0761, red markers) was stable during cooling to –70 °C and the subsequent heating to 110 °C, but transformed to cubic elemental aluminum (PDF 85-1327, green markers) at about 140 °C. At this temperature aluminum hydride and aluminum coexisted with mass fractions about 0.75 and 0.25, respectively. After further heating to 170 °C the dehydrogenation was completed.

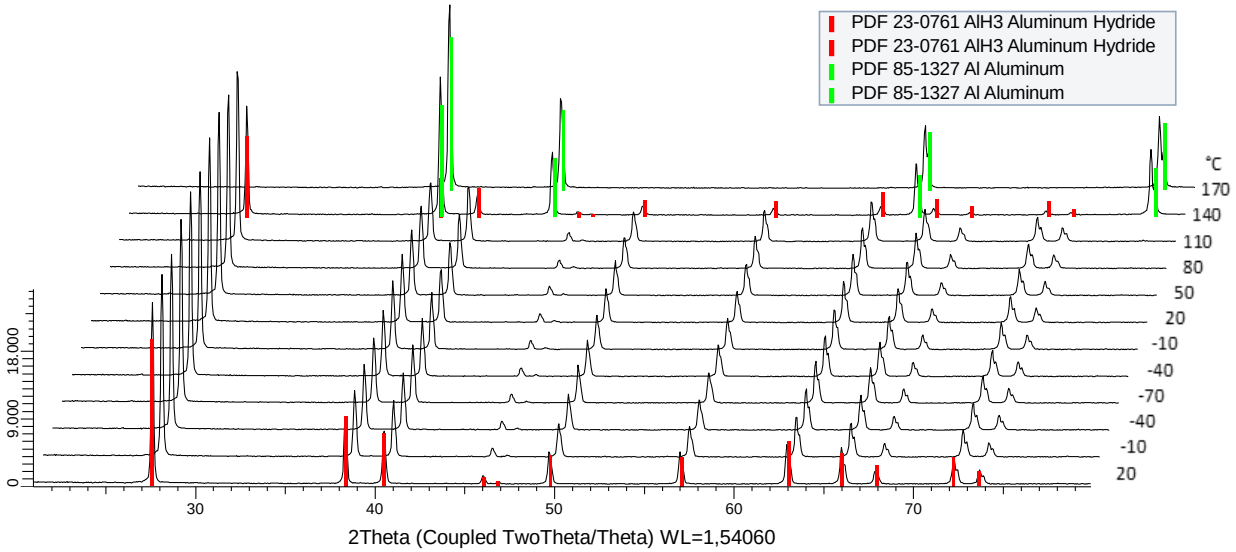

Figure 6: Waterfall plot of alane during cooling from 20 to –70 °C and subsequent heating to 170 °C, and markers of the α-AlH_3 (red) and cubic aluminum (green). Waterfall offset x = 10 % und y = 60 %.

The thermal expansion behavior of α-AlH_3 is shown in Figure 7, where lattice parameters, the cell volume, and the density obtained from Rietveld analysis were plotted versus temperature and evaluated using best fit straight lines. Resultant coefficients of thermal expansion (CTEs) and the density at room temperature were summarized in Table 1 and compared to values of a nanometer-sized aluminum (ALEX), micrometer-sized aluminum and aluminum oxide (corundum), samples were measured under the same conditions. The density of the α-AlH_3 amounts to 1.48 g/cm^3. Expectedly, the value is much lower than the densities of elemental aluminum and aluminum oxide with 2.70 and 3.99 g/cm^3, respectively. Furthermore, α-AlH_3 expanded highly anisotropically with CTEs of 1.25 10^{-5} K^{-1} along the lattice parameters a and b and 0.13 10^{-5} K^{-1} along c. Thus, the expansion in the plane stretched by the axis a and b was by a factor ten higher than along the axis c. The volume expansion however was moderate with

2.63 10^{-5} K^{-1} and lies between the values of the elemental aluminum samples and the aluminum oxides with 5.87, 6.48, and 1.38 10^{-5} K^{-1}, respectively (Table 1). Hence, densities and CTEs of aluminum are by the factors 1.8 and 2.2 higher than that of α-AlH_3. In the case of elemental aluminum, the nanometer-sized particles revealed slightly lower density and CTE values than the micron sized sample. Further details are reported elsewhere [9].

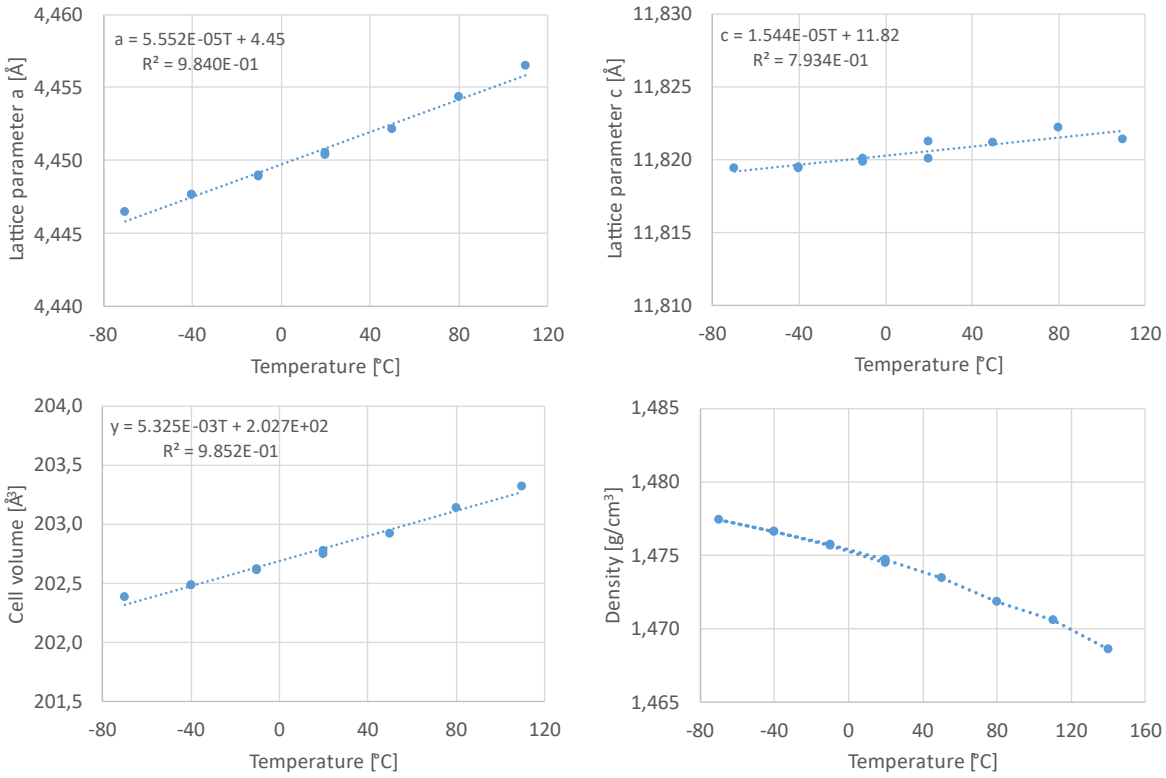

Figure 7: Lattice parameters a (top left.), c (top right), cell volume (bottom left) and density (bottom right) of α-AlH_3 measured during cooling and heating between –70 and 110 °C.

Table 1: Density and coefficients of thermal expansion of alane, aluminum and aluminum oxide.

Phase	Density @ RT	Coefficients of thermal expansion (CTEs) Lattice parameters		Elementary cell volume
		a	c	
	[g/cm³]	[10^{-5} K^{-1}]	[10^{-5} K^{-1}]	[10^{-5} K^{-1}]
α-AlH_3 (alane)	1.475	1.25	0.13	2.63
ALEX	2.695	1.95		5.87
Aluminum 18 µm	2.698	2.15		6.48
Aluminum oxide	3.985	0.44	0.49	1.38

A closer inspection of the diffraction series revealed an interesting detail. The intensive aluminum reflection at 75 °2θ was already present as weak peak in the background at the beginning of the measurement at 20 °C, and it gained intensity above110 °C (Figure 8). At this position, no reflection of aluminum hydride phase should appear. A reevaluated semi-quantitative phase analysis revealed 99.3 % α-AlH_3, 0.5 % δ-AlH_3, and 0.2 % elemental aluminum (Figure 9) at 20 °C. Besides, aluminum hydroxide may be present in a low concentration.

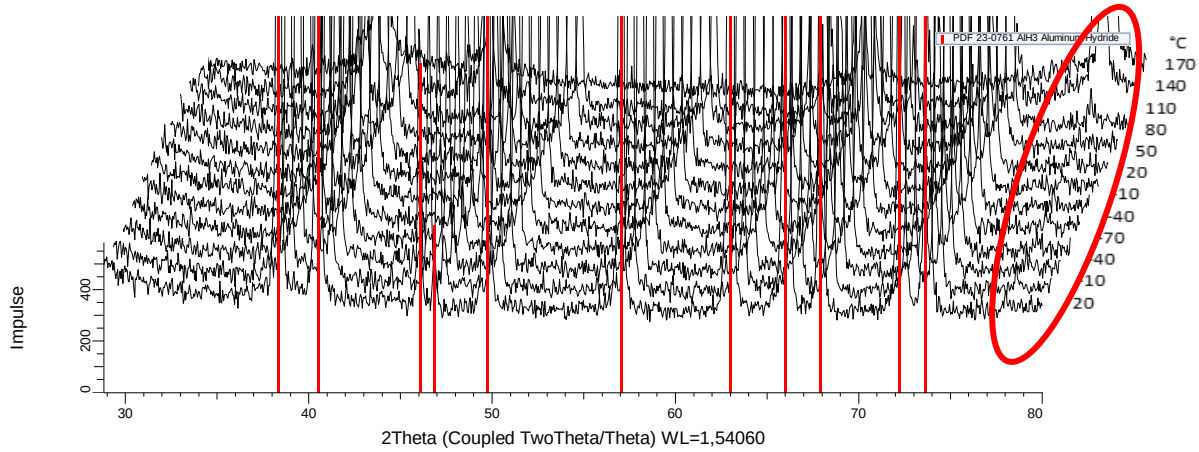

Figure 8: Enlarged view of the waterfall plot in figure 7. A small peak at 73 °2θ identifies elemental aluminum in the alane before the heating.

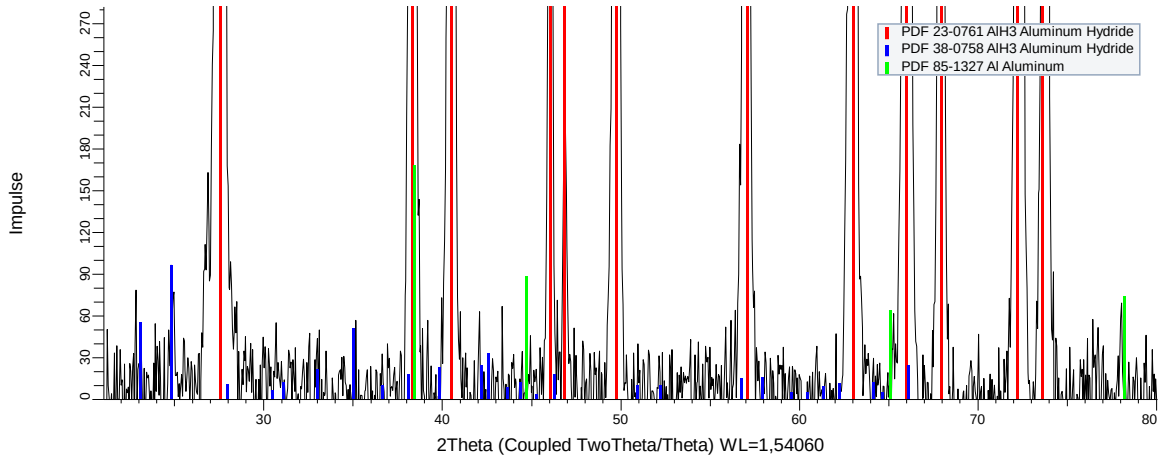

Figure 9: Enlarged view of a diffraction pattern of alane and phase analysis. Markers of α-AlH_3 (red, PDF 23-0761), δ-AlH_3 (blue, PDF 38-0758), and elemental aluminum (green, PDF 85-1327).

Monitoring the phase concentrations during quasistatic heating with five minutes relaxation time between the measurements and smaller temperature steps of 5 °C in the relevant

temperature range revealed a strongly delayed dehydogenation, which started at about 120 °C and dragged on over 50 °C and 250 minutes (Figure 10).

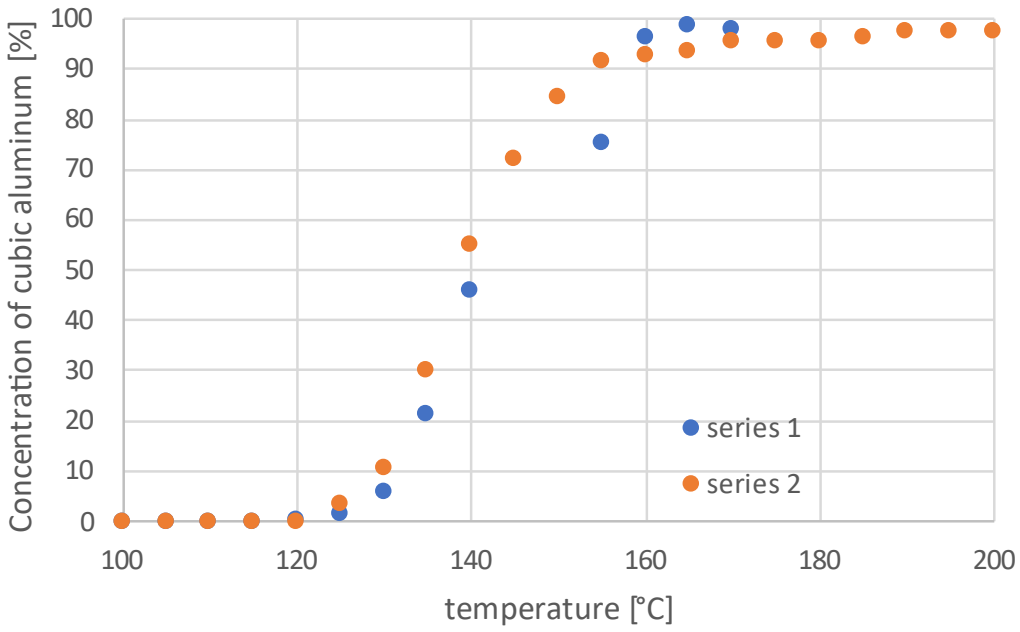

Figure 10: Concentration of cubic aluminum during heating alane from 100 to 200 °C.

Summary and conclusions

Aluminum hydride (alane) is a promising substance for rocket propellants and space applications. Re-investigations of a Russian product revealed interesting details and concepts for stabilization mechanisms. The investigations proved a surface-active stabilization, where decomposition starts at lattice defects, puncturing a stabilized surface. Subsequently, corrosion penetrates along defects, bulges fissure edges, and hollows out defective crystals until disappearance. Hence, crystallization of approximately defect-free crystals is a basic requirement for a stable product. No hints to a stabilizing additive, such as magnesium, were found in the samples, but some oxygen by means of EDX. The investigations with X-ray diffraction identified the expected α-AlH_3 with traces of a polymorph (0.5%), but also 0.2% elemental aluminum. Hence, beside the frequently discussed stabilization concept of an aluminum oxide or hydroxide layer (or both), a thin epitaxial elemental aluminum layer may protect the crystals from decomposition, most like with a very thin aluminum oxide layer on

top, which is known to protect elemental aluminum from further oxidation. Further on, the investigations showed that the alane started to dehydrogenate under nitrogen flushing to elemental aluminum at 120 °C, and that the transition dragged on over 50 °C and 250 minutes. The slow kinetic of the dehydrogenation may help to create a very thin closed aluminum layer on aluminum hydride crystals in nitrogen, which could be stabilized afterwards by gradual addition of oxygen. For a thermal treatment, however, the anisotropic expansion behavior of the α-AlH_3, and significantly varying CTEs of the bulk and potential layers, and the anisotropic expansion of the alane should be considered to avoid surface fracturing or delamination. CTEs of α-AlH_3 amounted to 0.13, 1.25, and 2.63 10^{-5} K^{-1} for the lattice parameter a, c, and the cell volume, respectively.

Abbreviations

AlH_3	aluminum hydride, alane
ALEX	nanosized aluminum
CTE	Coefficients of thermal expansion
EDX	energy dispersive X-ray spectroscopy
GAL-2	alane sample
ICDD	International Centre for Diffraction Data, Newtown Square, PA, USA
ICT	Fraunhofer Institute for Chemical Technology, Pfinztal, Germany
PDF	powder diffraction file of the ICDD
SEM	scanning electron microscopy
SDD	silicon-drift detector
XRD	X-ray diffraction

References

[1] V. Thome, P. B. Kempa, M. Herrmann, Aluminiumhydrid AlH_3 – Literaturübersicht und Eingangskontrolle.: Technische Mitteilung 2031205_10, T/R430/3A001/K1110, Fraunhofer ICT, Pfinztal, Deutschland, **2003**.

[2] J. Graetz, J. J. Reilly, V. A. Yartys, J. P. Maehlen, B. M. Bulychev, V. E. Antonov et al., Review: Aluminum hydride as a hydrogen and energy storage material: Past, present, and future, *Journal of Alloys and Compounds* 509 (**2011**) 517-528.

[3] Z. El Sayah, R. Brahmi, R. Beauchet, Y. Batonneau, C. Kappenstein, Synthesis, characterization and treatment of alane (aluminum hydride, AlH3), Proc. *7th European Conference for Aeronautics and Space Sciences*, Milano, Italy, July 3-6, **2017**.

[4] H. Liu, L. Zhang, H. Ma, C. Lu, H. Luo, X. Wang et al., Review: Aluminum hydride for solid-state hydrogen storage: Structure, synthesis, thermodynamics, kinetics, and regeneration, *Journal of Energy Chemistry* 52 (**2021**) 428-440.

[5] Wikipedia, Aluminiumhydrid, [April **2021**], https://de.wikipedia.org/wiki/Aluminiumhydrid.

[6] L. Petrini, Synthesis, stability, and properties of TNO's aluminum hydride, *Tesi di Laurea*, Politecnico di Milano, Facoltà die Ingegneria Industriale, **2012**.

[7] V. Thome, P. B. Kempa, M. Herrmann, Structure, Chemical and Physical Behavior of Aluminum Hydride, *Energetic Materials - Reaction of Propellants, Explosives and Pyrotechnics*, Karlsruhe, Germany (**2003**) 104.1-12.

[8] P. B. Kempa, V. Thome, M. Herrmann, Structure, Chemical and Physical Behavior of Aluminum Hydride, *Part. Part. Syst. Charact.* 26 (**2009**) 132–137.

[9] M. Herrmann, P. B. Kempa, U. Förter-Barth, H. Weyrauch und M. Juez Lorenzo, Untersuchungen zur Stabilisierung von Aluminiumhydrid, Bericht, September 2021, Fraunhofer ICT, Pfinztal, Deutschland

[10] R. A. Young (Ed.), The Rietveld method: Product of the International Workshop on the Rietveld Method in Petten, The Netherlands, June 13–15, 1989, Oxford University Press, Oxford, **1993**.

[11] Bruker AXS, TOPAS-32 V6, User manual, Karlsruhe, Germany.

[12] J. W. Turley, Aluminiumhydrite, private communication, PDF-2, **1999**.